Journal of Applied Electrochemistry **34**: 315–321, 2004.

Electrodeposition, composition and structure of Zn–Cr alloys

Tz. BOIADJIEVA[1], D. KOVACHEVA[2], K. PETROV[2], S. HARDCASTLE[3], A. SKLYAROV[3] and M. MONEV[1,*]
[1]*Institute of Physical Chemistry, Bulgarian Academy of Science, 1113 Sofia, Bulgaria*
[2]*Institute of General and Inorganic Chemistry, Bulgarian Academy of Science, 1113 Sofia, Bulgaria*
[3]*University of Wisconsin Milwaukee, Advanced Analysis Facility, Milwaukee, WI 53201, USA*
*(*author for correspondence, e-mail: monev@jpchp.jpc.bg)*

Received 13 October 2002; accepted in revised form 31 March 2003

Key words: cyclic voltammetry, electrodeposition, X-ray diffraction, X-ray photoelectron spectroscopy, Zn–Cr alloys

Abstract

The effect of polyethylene glycol (PEG 1500) as additive and of deposition conditions on Zn–Cr alloy electrodeposition from an acidic sulfate electrolyte at room temperature, without agitation was investigated. PEG polarizes the overall cathodic reaction and inhibits Zn deposition. Cr codeposition with Zn starts at a cathodic potential of about −1,95 V vs Hg/Hg_2SO_4, which is reached at current density of about 20 A dm^{-2} in galvanostatic conditions. Zn–Cr alloy coatings containing up to 28 at % Cr were obtained depending on the plating conditions. SEM observations showed an island-like structure, formed by the local growth of crystals, which covered the surface during further deposition. In the first stages of electrodeposition the powder diffraction spectra contain lines of b.c.c. Γ-(Zn,Cr) phase ($a_\Gamma \approx 3.02$ Å). After 30 s deposition time weak lines of Zn-based η phase ($a_\eta \approx 2.67$ Å, $c_\eta \approx 4.90$ Å) appear, and become clearly visible in coatings deposited for 90 s. The average Cr content in the alloy coatings decreases with advancing deposition. The as-plated surface contains C in organic compounds and $Zn(OH)_2$. After 50 min sputtering, Zn and a mixture of Cr, Cr_2O_3 and Cr_7C_3 were found. The presence of organic C and O, probably from inclusions of PEG, were also detected.

1. Introduction

Codeposition of Zn with a number of metals (Co, Ni, Fe, Mn, Sn) improves some physico-mechanical properties of the coatings as well as their corrosion resistance. Zn–Co, Zn–Ni and Zn–Fe alloy coated steel sheets are utilized in various industries including automotive, electric appliance and building materials [1, 2]. Recently, attention has been paid to the electrodeposition of Zn–Cr alloy coatings [3, 4]. Several patents claim preparation of Zn–Cr alloy deposits with excellent corrosion resistance, containing 5–40 mass % Cr from trivalent Cr based electrolytes [5–10]. However, the deposition of alloy coatings from such electrolytes is associated with some difficulties caused by the complex chemistry and electrochemistry of Cr(III) species in aqueous solutions. It has been reported that Cr and Zn do not codeposit readily in the absence of certain additives. Polyoxyalkylene compounds [5, 7, 8], non-ionic organic additives, each having at least a triple bond [6], polyethyleneoxyphenol derivatives [10], O-compounds group colloids [11], urea [12, 13] and glycine [14, 15] all induce the codeposition of Cr with Zn.

Data on Zn–Cr deposition are various. Addition of polyethylene glycol (PEG) with high molecular mass permits deposition of Zn–Cr alloy coatings of good quality [16, 17]. Electrolytes, containing PEG of low molecular mass (n = 3–60) are also proposed [5]. Some patents report deposition of alloy coatings containing up to 40 mass % Cr at temperatures ranging from 40 to 60 °C [5–10], while other authors claim that the increase in the temperature reduces the current efficiency and the Cr content in the alloy [13]. The deposition of the alloy is also affected by the intensity of the electrolyte stirring and electrolyte pH. In some patents [5, 7, 9] the relative flow rate of the electrolyte is specified to be 1–2 m s^{-1} while in other experiments vertical cathode movement is applied [13] or the coatings are deposited without stirring [16, 17]. The current density (*c.d.*) and pH also vary in wide intervals 5–300 A dm^{-2} and pH 1–4, respectively.

Data on the composition and structure of intermetallic phases formed in the galvanic Zn–Cr system are scarce and rather inconsistent, probably due to the different deposition conditions. The hexagonal η-(Zn,Cr) phase and θ-(Zn,Cr) phase (a = 12.89 Å,

$c = 30.5$ Å) containing 3.8–7.0 mass % Cr as well as a Cr phase are formed at thermal equilibrium [18]. The η-(Zn,Cr) phase coexists with several unidentified and probably nonequilibrium Zn–Cr phases in galvanic Zn–Cr coatings [5, 11, 19]. Detailed analyses reveal the existence of η-(Zn,Cr) phase ($a = 2.66$–2.74 Å, $c = 4.61$–4.95 Å, depending on composition), containing up to 15 mass % Cr [5]. In the concentration interval from 5–10 to 30 mass % Cr, δ-(Zn,Cr), hexagonal ($a = 2.72$–2.78 Å, $c = 4.43$–4.60 Å) and Γ-(Zn,Cr), b.c.c. ($a = 3.00$–3.06 Å) crystallize. These phases could develop singly or coexist in the coating, depending on deposition conditions [5]. Recently, it has been reported that Zn–Cr alloy coatings containing under 20 and 35–40 mass % Cr have h.c.p. and b.c.c. phases, respectively, while in coatings containing 20–35 mass % Cr the two phases coexist [20]. X-ray diffraction (XRD) measurements of vapour deposited Zn–Cr alloys also show a gradual change in structure as the Cr concentration increased, from the hcp characteristic of Zn to a metastable bcc structure [21].

The chemical state of Cr in electroplated Zn–Cr alloy coatings was studied by X-ray photoelectron spectroscopy (XPS) [16, 17]. It was found that PEG with molecular mass higher than 1540 polarized the deposition potential of Zn to the reduction potential of Cr thus permitting the codeposition of metallic Cr, while Cr(III) was present in the deposits obtained from PEG-free and PEG 200 containing baths.

The aim of the present work was to investigate the electrodeposition conditions on the codeposition of Cr with Zn from acidic sulfate electrolyte containing PEG 1500, at room temperature, without agitation, and to study the composition and the structure of the alloy coatings.

2. Experimental details

Zn–Cr alloy deposits were obtained from a sulfate electrolyte at 25 °C, pH 1.6 (adjusted by adding sulfuric acid), without agitation:

Electrolyte composition:

$ZnSO_4 \cdot 7H_2O - 172.5\,g\,l^{-1}$

$Cr_2(SO_4)_3 \cdot 18H_2O - 143.2\,g\,l^{-1}$

$Na_2SO_4 - 71.0\,g\,l^{-1}$

PEG 1500 ($0.5\,g\,l^{-1}$) was used as an additive.

All compounds used were of analytical grade. Chromium(III) sulfate was prepared through reduction of CrO_3 with ethanol in sulfuric acid medium.

The effect of conditions on Zn–Cr codeposition was studied by cyclic voltammetry. A thermostated 50 ml three-electrode electrochemical cell containing a Hg/Hg_2SO_4 reference electrode, a Pt counter and a Pt working electrode (a Pt wire with area of 0.16 cm^2) was used. The scan rate was 25 mV s^{-1}. The investigations were performed with a model 263A potentiostat/galvanostat (EG&G Princeton Applied Research).

Zn–Cr alloys were deposited under galvanostatic conditions onto Pt and steel substrates with dimensions 20 mm × 10 mm (*c.d.* ranging from 20 to 70 A dm^{-2}).

The content of Cr in the coatings was determined by electron probe X-ray microanalysis (EDX) (JCXA 733 Jeol, Japan). The morphology of the alloy coatings was observed by scanning electron microscopy (SEM) (JSM 5300, Jeol, Japan).

XRD patterns of galvanic coatings deposited on Pt and steel substrates were recorded with an automatic powder diffractometer type DRON using Bragg-Brentano geometry, CuK_α filtered radiation and scintillation counter. Diffraction data were collected in the angular interval 10–125° (2θ) in a step-scanning mode, at steps of 0.02° (2θ) and counting time of 5 s per step. Unit cell parameters were calculated from the high angle diffraction lines. Instrumental corrections were introduced using the reflections of the Pt substrate as an internal standard. The film thickness t was calculated from the integral intensity I_c of the (200) peak of the Pt substrate, recorded at several low glancing angles γ whose values varied from 5 to 15° (θ) (glancing – incidence geometry [22]), according to Equation 1:

$$\ln I_c = \ln I_0 - \mu^* t \frac{\sin\gamma + \sin(2\theta - \gamma)}{\sin(2\theta - \gamma)\sin\gamma} \quad (1)$$

where I_c is the integral intensity corrected for deviation from Bragg–Brentano geometry, μ^* the mean linear absorption coefficient, and θ the Bragg angle.

The surface chemical state of the Zn–Cr alloy was investigated by means of XPS. An HP 5950A ESCA spectrometer with a monochromatic AlK_α source was used. An Ar ion source was used to sputter the sample at 4.5 keV with a rate of 1.5 nm min^{-1}. The XPS data were calibrated using the adventitious C 1S line set to 285.0 eV in binding energy (BE).

3. Results

3.1. *Electrochemical investigations*

The voltammogram in the absence of an additive indicates that along with the anodic maximum for Zn there appears another very small maximum, which is referred to trans-passive Cr dissolution at 0.65 V (Figure 1). The PEG additive polarises the overall cathodic reaction and inhibits Zn deposition, thus further stimulating Cr codeposition, the latter being detected from the increased anodic maximum at 0.65 V. These results are confirmed by EDX analysis of samples obtained under galvanostatic conditions. An additive-free electrolyte produces deposits with Cr content less

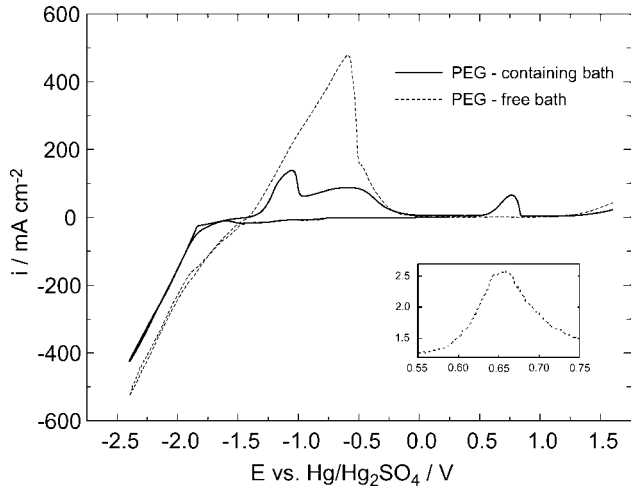

Fig. 1. Effect of PEG on Zn–Cr electrodeposition.

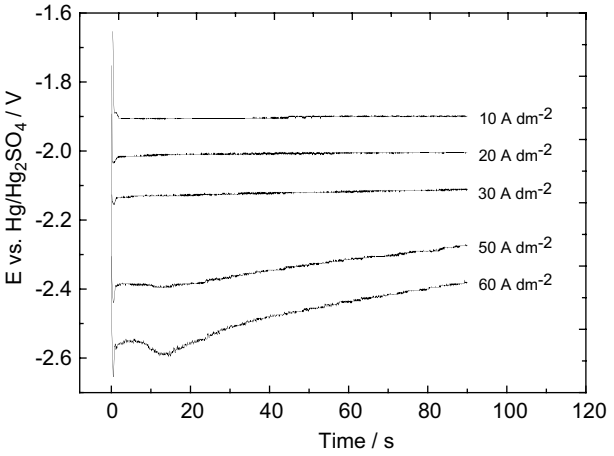

Fig. 3. Potential–time plots for Zn–Cr electrodeposition under different *c.d.*

than 1 at %, while analysis of the coatings deposited in the presence of PEG indicated that the Cr content increased to about 28 at %.

Voltammograms to various cathodic switching potentials show that Cr codeposition starts when the cathodic potential reaches values of about −1.95 V (Figure 2), that is, with high polarization. Regardless of the different experimental conditions, this value is close to the potentials reported by other authors for the start of codeposition of metallic Cr with Zn [11, 13], as well as the value of the nucleation potential of Cr from commercial trivalent electrolyte [23]. A shift of the cathodic switching potential to more negative values leads to an increase in both the Zn and the Cr anodic maxima. The anodic maxima could be assigned to a dissolution, not of pure metals, but of Zn–Cr phases. The elucidation of the character of these peaks will be the subject of further investigations.

The potential against time plots, recorded under galvanostatic conditions, reveal that the codeposition potential of Cr is reached at a *c.d.* of about 20 A dm^{-2} (Figure 3). The coatings deposited at this value of *c.d.* for 180 s contain 0.5 at % Cr. With an increase in cathodic *c.d.* the Cr content increases from about 13 at % to about 24 at % at 30 A dm^{-2} and 50 A dm^{-2}, respectively. With *c.d.s* exceeding 50 A dm^{-2}, the alloy coatings become rough, the latter being reflected in the course of the potential against time plots.

Further investigations were carried out with samples deposited mainly at 50 A dm^{-2}.

Figure 4 illustrates a potential against time plot of galvanostatic stripping of a Zn–Cr deposit obtained for 5 s. Two distinct steps are recorded at potentials corresponding to the dissolution potentials of pure Zn and Cr coatings. This may imply that the electroplating begins with simultaneous deposition of both metals. The

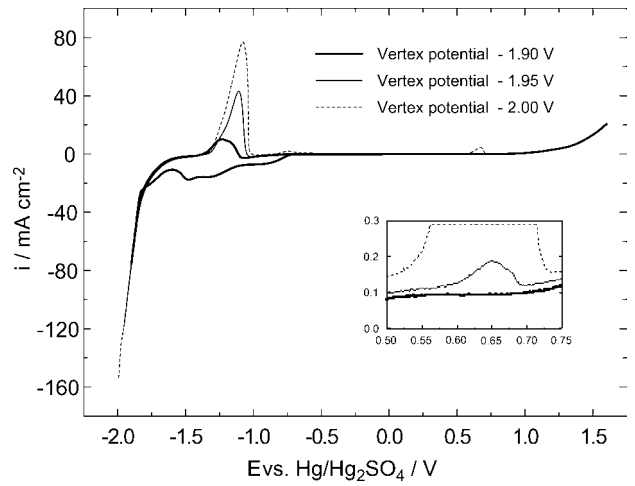

Fig. 2. Effect of varying the vertex potential on Zn–Cr electrodeposition.

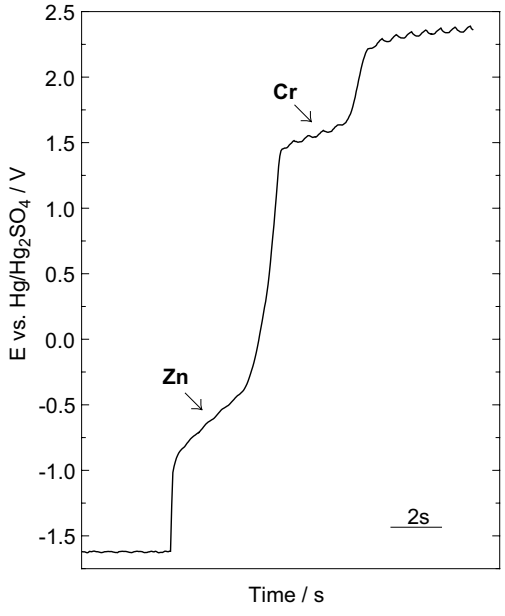

Fig. 4. Anodic chronopotentiogram of Zn–Cr deposit (obtained at 50 A dm^{-2} for 5 s) by galvanostatic stripping at 7 A dm^{-2} in 1 M Na_2SO_4.

mechanism of alloy dissolution is more complicated and will be the subject of further discussion.

3.2. *Morphology*

SEM observations of Zn–Cr coatings, deposited for different times show an island structure, formed by the local growth of crystals, which covered the surface during further deposition (Figure 5(a), (b) and (c)).

The average Cr content in samples deposited for 5–15 s is about 28 at %. The island-like formations are composed of Zn and 31 at % Cr. The substrate is covered with a thin film incorporating a number of very small 'islands'. The Cr content in this film is 18–23 at %. With longer deposition time (90 s), the average Cr content is reduced to about 24 at %.

The results, however, do not reflect the true composition of the deposits since the EDX analysis does not give information about oxygen and carbon content.

3.3. *Phase composition*

The Zn–Cr coatings are relatively thin having a thickness of about 1 to 5 μm. Thus their XRD characteristics should be regarded as integral ones, averaged over the whole irradiated volume.

XRD patterns of samples deposited at 50 A dm^{-2} for 10 and 30 s, (Figure 6(a) and (b)), contain lines of the Pt substrate and of Γ-(Zn,Cr) alloy. Coatings deposited for 30 s also exhibit the presence of η-Zn phase, but the corresponding lines are distinctly visible in coatings deposited for longer periods (Figure 6(c)). The average unit cell parameter a_Γ of the Γ-phase increases with increasing deposition time at fixed *c.d.* At fixed deposition time, a small decrease of a_Γ is observed with decreasing *c.d.*

The dependence of a_Γ on the relative atomic Cr content x in the Γ-phase is *a priori* unknown. However, some meaningful information about x could be extracted if a_Γ is assumed to vary linearly with x between the corresponding values for a hypothetical b.c.c. Zn phase $(a_{Zn})_{bcc} = 2(a_{Zn})_{hcp}/\sqrt{3} = 3.077$ Å and that for the b.c.c. Cr phase $(a_{Cr})_{bcc} = 2.885$ Å. The variation of x determined from this linear plot (Figure 7) enables us to draw some conclusions.

The average relative Cr content x in the Γ-phase formed at the initial stages of deposition is about 33 at %. Data from EDX analysis of the island-like formations (Figure 5(a)), which are suggested to be mainly built-up of Γ-phase, are also very close. With advancing deposition, the value of x in the Γ-phase gradually decreases to the average value of 27 at %.

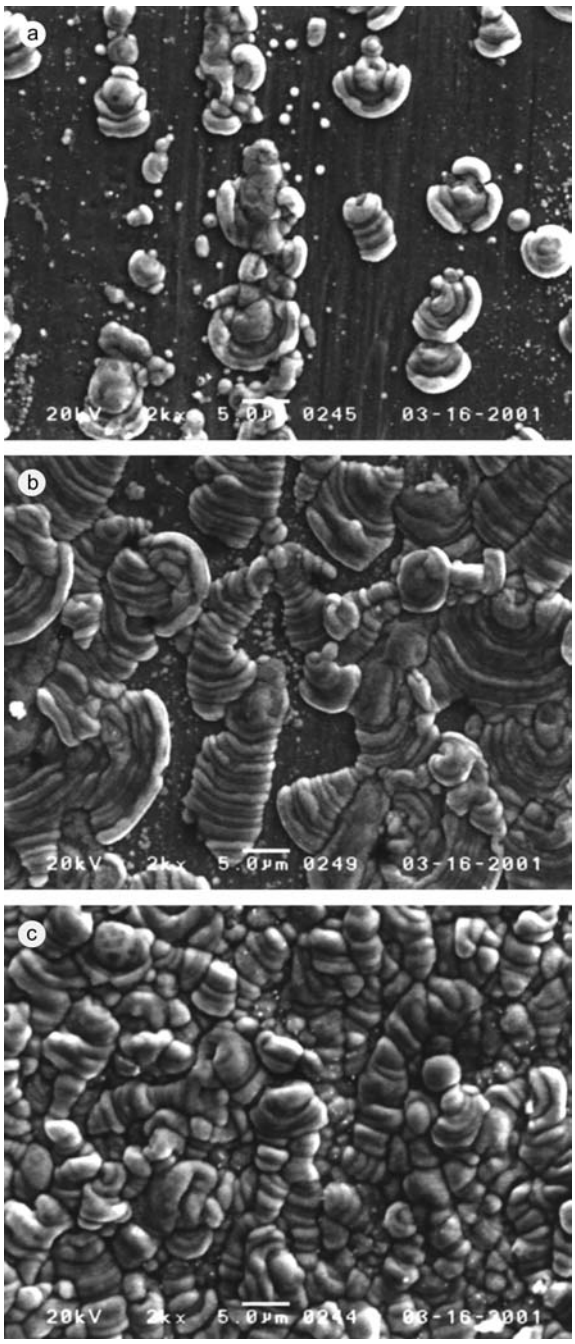

Fig. 5. SEM images of Zn–Cr alloy. Deposition time: (a) 5 s, (b) 15 s, (c) 90 s. Current density 50 A dm^{-2}.

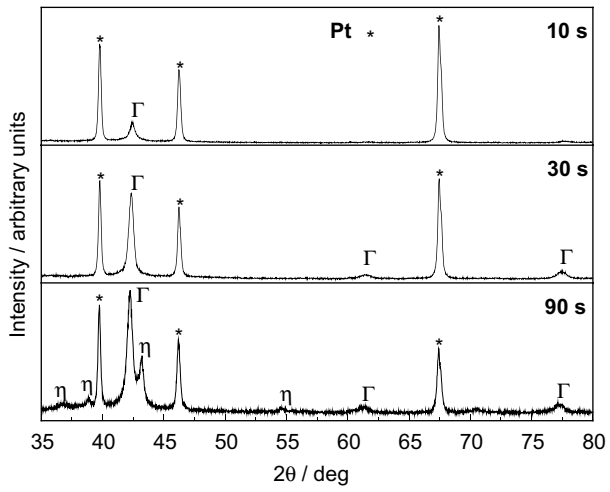

Fig. 6. XRD patterns of Zn–Cr samples deposited at 50 A dm^{-2} for different time on Pt.

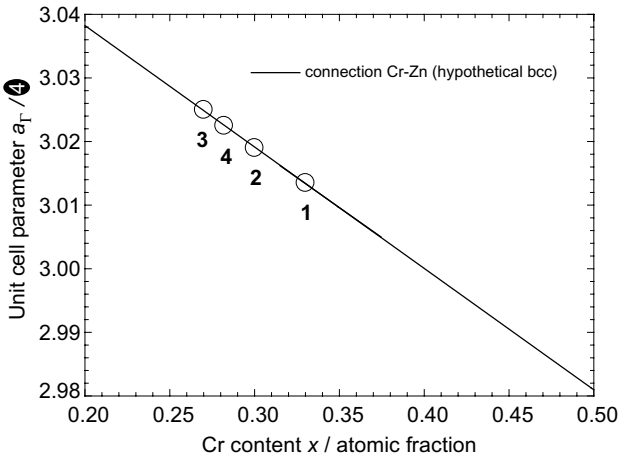

Fig. 7. Hypothetical dependence of the lattice parameter a_Γ of the Γ-phase from the atomic Cr content x. Deposition time: (1) 10 s, (2) 30 s, (3) 90 s, *c.d.* 50 A dm^{-2}; (4) 90 s, *c.d.* 30 A dm^{-2}.

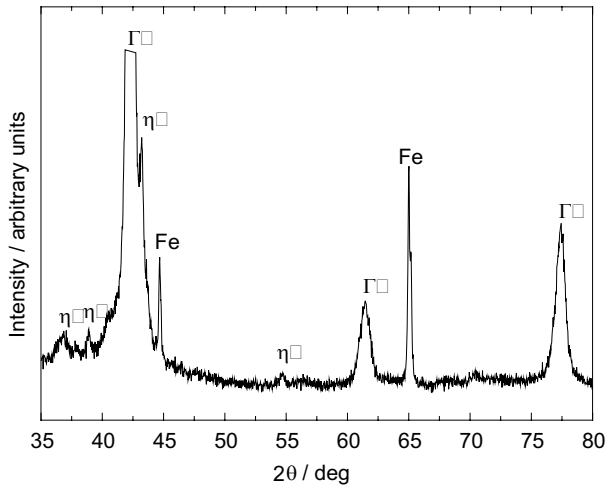

Fig. 8. XRD pattern of Zn–Cr sample deposited at 50 A dm^{-2} for 90 s on steel.

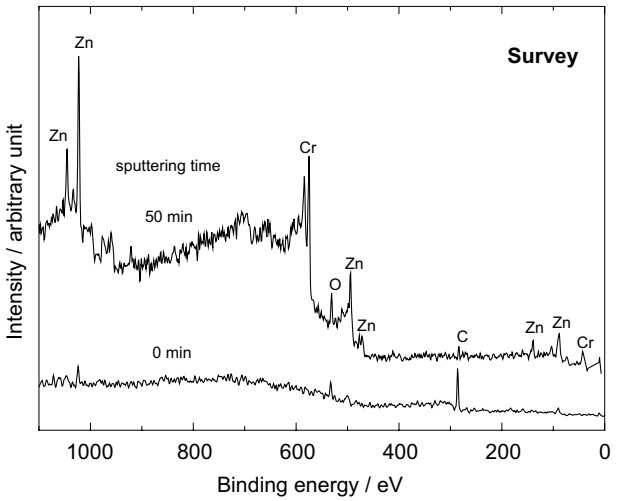

Fig. 9. XPS spectra of Zn–Cr alloy coating.

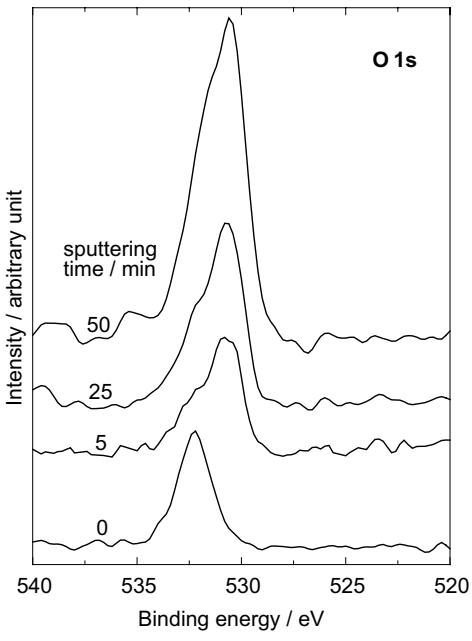

Fig. 10. O 1s spectra of Zn–Cr alloy coating.

The presence of η-Zn phase in samples deposited for short times is very likely, but in amounts too small to be recorded by XRD. The lower Cr content in the film incorporating the small island-like formations provides indirect evidence of this. Crystallization of the η-Zn phase also seems to occur when the Cr content in the Γ-phase is reduced below the critical value of 27 at %. Taking into account the island-like structure of the coatings, it can be suggested that Cr depleted Γ-phase and the η-Zn phase are formed at the grain boundaries and on the surface of the coating.

The decrease of Cr content in the Γ-phase and the increase in the relative share of the η-Zn phase, with increasing deposition time, is probably due to changes occuring near the cathode. An increase in pH as a result of hydrogen evolution leads to production of oligomeric olated species and to reduction of the electroactive Cr species [24]. This fact is in agreement with investigations on Cr electrodeposition from trivalent Cr-based electrolytes in which a decrease in the plating rate with increasing plating time is found [24–27].

XRD patterns of samples deposited on steel, similar to these deposited on Pt, contain lines of the Γ-(Zn,Cr) phase and of the η-Zn phase (Figure 8). This supposes analogy in the process of deposition on both substrates.

3.4. *Surface chemical state*

The XPS survey scans for the as is (non sputtered) and for 50 min sputtered sample (obtained at 50 A dm^{-2} for 90 s) are shown in Figure 9. In addition to the usual adventitious carbon, only Zn and O are seen on the surface prior to sputtering. From the O 1s region scans, the surface O can be identified as a mixture of organic oxides (532 eV) and Zn oxy-hydroxide (531 eV), (Figure 10). After sputtering, the O 1s peak shifts to lower BE's associated with Zn or Cr oxides (530 eV). A small contribution from organic fragments can be seen in the O 1s spectra after 50 min sputter. The C 1s spectra

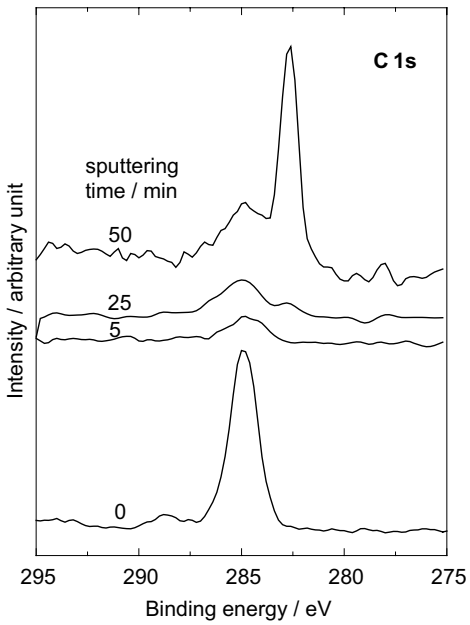

Fig. 11. C 1s spectra of Zn–Cr alloy coating.

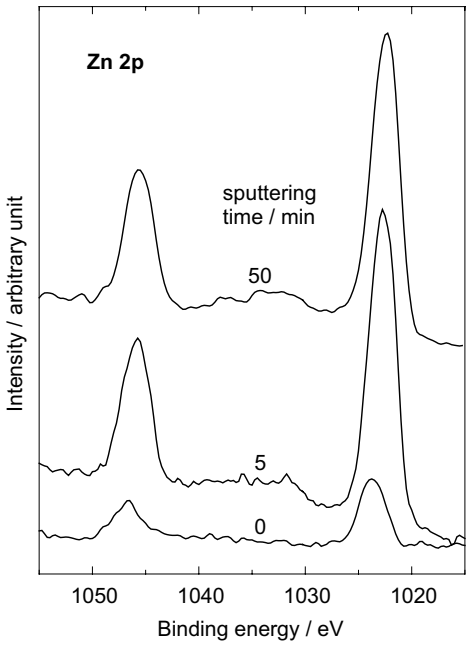

Fig. 12. Zn 2p spectra of Zn–Cr alloy coating.

(Figure 11) shows a large adventitious peak at 285 eV and a smaller peak close to 289 eV associated with C double bonded with O in organic fragments. After 5 min sputter the adventitious C is greatly reduced as well as the C═O component. The 50 min sputter shows a new peak near 282.8 eV. A carbon peak with a similar BE is measured with thermally treated Cr deposited from Cr(VI) electrolyte containing formic acid [28, 29]. This peak is assigned to the formation of chromium carbide (Cr_7C_3). The same BE peak is measured from Cr coatings deposited from sulfate electrolytes containing oxalate and also was identified as chromium carbide [30, 31]. The initial Zn 2p 3/2 peak increases substantially after the 5 min sputter and the peak shifts slightly to lower BE. Further sputtering causes little change in the intensity or the peak position (Figure 12). After 50 min sputter, the Zn LMM Auger peak position is near 496 eV (Figure 9). This position indicates metallic Zn is present. The analysis of the Cr spectra is complicated by the gettering of oxygen on to freshly s gen in the HP XPS chamber makes the analysis of Cr/Cr oxides difficult. However, several observations can be made. Prior to sputtering the surface shows the presence of very little Cr (Figure 13). After 5 and 25 min sputtering time, two Cr 2p 3/2 peaks start to grow. One is near 576 eV and can be identified as Cr_2O_3. The second Cr peak has a BE at 572.5 eV and after sputtering for 50 min is by far the largest Cr peak.

From the measured C 1s carbide peak and the overall elemental composition (Table 1) the 572.5 eV peak can be assigned to Cr_7C_3 compound. Sputtered Cr metal only shows a tendency to form chromium carbide on the surface after sputtering. However, the carbide peak in Figure 13 (50 min sputter) is higher than the authors have seen from Cr metal sputtered in the HP chamber. From Table 1, most of the oxygen present after 50 min

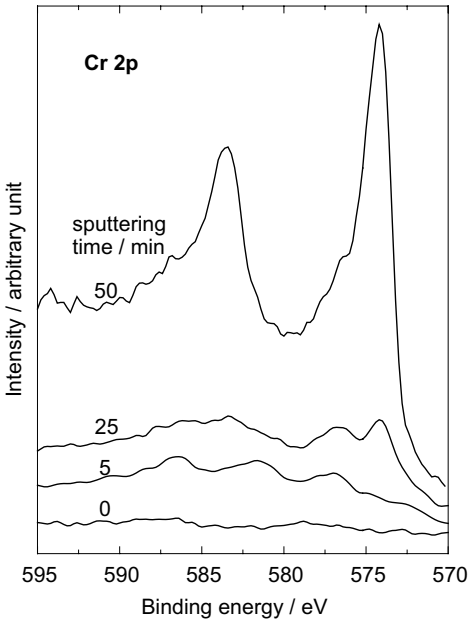

Fig. 13. Cr 2p spectra of Zn–Cr alloy coating.

Table 1. Surface composition

Sputter time /min	Zn /at %	Cr	O	C
0	21	little	79	*
5	45	4	40	11
25	38	15	37	10
50	24	27	32	17

* most of the C on the surface is adventitious.

sputter is thought to be gettered oxygen attached to the Cr.

4. Conclusions

The PEG additive polarises the overall cathodic reaction and inhibits Zn deposition. The codeposition of Cr with Zn starts at a cathodic potential of about −1.95 V, which is reached at *c.d.* of about 20 A dm^{-2} in galvanostatic conditions. Zn–Cr alloy deposits containing up to 28 at % Cr were obtained depending on the plating conditions.

The alloy coating is formed by the local growth of crystals, building an island-like structure, which covers the surface during further deposition.

In the first stages of electrodeposition the Zn–Cr alloy deposits are mostly composed of Cr-based Γ-phase ($a_\Gamma \approx 3.02$ Å) containing about 33 at % Cr. With advancing deposition the relative Cr content in the Γ-phase gradually decreases to a critical average value of 27 at % and the relative share of the η-Zn phase ($a_\eta \approx 2.67$ Å, $c_\eta \approx 4.90$ Å) increases. As a result the average Cr content in the alloy gradually decreases.

The as-plated surface of the alloys contains C in organic compounds and $Zn(OH)_2$. After 50 min sputter, Zn and mixture of Cr, Cr_2O_3 and Cr_7C_3 are found. The presence of organic C and O, originating most probably from inclusions of PEG, is also registered.

Acknowledgements

This work was supported by the National Scientific Research Fund under Project X-816. The authors are indebted to Dr Vitkova for fruitful discussions and wish to express their gratitude to Ms Tsacheva for the EDX analysis.

References

1. W. Siegert and J. O'Grady, *Metalloberfläche* **47** (1993) 378.
2. V. Leroy, Galvatech '95, 'The Use and Manufacture of Zinc and Zinc Alloy-coated Sheet Steel Products into the 21st Century, Conference Proceedings, Chicago, IL, 17–21 Sept. (1995), p. 279.
3. Y. Miyoshi, H. Odashima, Y. Shindo, M. Yoshida and T. Kamanaru, Nippon Steel Technical Report No. 57, 16–21 Apr. (1993) p. 16.
4. T. Ichida, Galvatech '95, *op. cit.* [2], p. 359.
5. *US Patent 4 877 494*, *EP 0 285 931 A1*, *US Patent 4 897 317*.
6. *US Patent 5 273 643*.
7. *US Patent 5 510 196*, *EP 0 607 452 A1*.
8. *EP 0 638 668 A1*.
9. *EP 0 643 157 A1*.
10. *US Patent 5 616 232*.
11. A. Takahashi, Y. Miyoshi and T. Hada, *J. Electrochem. Soc.* **141** (1994) 954.
12. *Russian Patent 328 208*.
13. A. Watson, Y.J. Su, M.R. El-Sharif and C.U. Chisholm, *Trans. Inst. Met. Finish.* **71**(1) (1993) 15.
14. N.B. Berezin, N.V. Gudin, V.V. Chevela and A.G. Filippova, *Zashtita metallov* **28**(6) (1992) 961.
15. N.B. Berezin, N.V. Gudin, A.G. Filippova, E.A. Matulenis and Yu. V. Borisov, *Zashtita metallov* **29**(1) (1993) 99.
16. T. Ohgai, J.S. Ki, T. Akiyama and H. Fukushima, *The Minerals, Metals & Materials Society* (1998) 225.
17. T. Akiyama, S. Kobayashi, J. Ki, T. Ohgai and H. Fukushima, *J. Appl. Electrochem.* **30** (2000) 817.
18. M. Hansen and Ê. Anderko, 'Constitution of Binary Alloys', Metallurgizdat, Moscow (1962) p. 605.
19. M.R. El-Sharif, C.U. Chisholm, Y.J. Sut and L. Feng, 'Advances in Surface Engineering', Vol. 1 (Royal Society of Chemistry, 1997), p. 95.
20. M. Miyake, T. Hirato, E. Matsubara and Y. Awakura, Second International Conference on 'Processing Materials for Properties', San Francisco, CA, 5–8 Nov. (2000), p. 779.
21. L. Guzman, M. Adami, W. Gissler, S. Klose and S. De Rossi, *Surf. Coat. Technol.* **125** (2000) 218.
22. I.C. Noyan, T.C. Huang and B.R. York, *Critical Reviews in Solid State and Mater. Sci.* **20**(2) (1995) 125.
23. J.N. Howarth and D. Pletcher, *J. Appl. Electrochem.* **18** (1988) 644.
24. T. Pearson and E. Long, *Trans. Inst. Metal Finish.* **76**(6) (1998) B83.
25. I. Drela, J. Szynkarczyk and J. Kunicki, *J. Appl. Electrochem.* **19** (1989) 933.
26. A.M. Smith, A. Watson and D.H. Vaughan, *Trans. Inst. Metal Finish.* **71**(3) (1993) 106.
27. Zh. Tu, Zh. Yang, J. Zhang, M-Zh. An and W-L. Li, *Plat. Surf. Finish.* Nov. (1993) 79.
28. S. Hoshino and G.B. Hoflund, *JES* **133**(4) (1986) 681.
29. G.B. Hoflund, D.A. Asbury, S.J. Babb, A.L. Grogan, Jr., H.A. Laitinen and S. Hoshino, *J. Vac. Sci. Technol. A* **4**(1) (1986) 26.
30. E.N. Lubnin, A.A. Edigaryan and Yu. M. Polukarov, *Protection of Metals* **36**(4) (2000) 301.
31. V.A. Safonov, L.N. Vykhodtseva, A.A. Edigaryan, A.D. Aliev, E.B. Molodkina, A.I. Danilov, E.N. Lubnin and Yu. M. Polukarov, *Russ. J. Electrochem.* **37**(2) (2001) 127.